Development and application of a multicompartmental model to study very low density lipoprotein subfraction metabolism

C. J. Packard,[1] A. Gaw,* T. Demant,† and J. Shepherd

Institute of Biochemistry, Glasgow Royal Infirmary, Glasgow, G4 OSF, UK; Department of Molecular Genetics,* University of Texas, Southwestern Medical Center, 5323 Harry Hines Boulevard, Dallas, TX 75235; and Institut für Klinische Chemie,† Klinikum Grosshadern, Marchioninistrasse, 81366 München, Germany

Abstract A multicompartmental model has been devised to explain apolipoprotein B (apoB) kinetics in very low density lipoprotein subfractions (VLDL$_1$ S$_f$ 60–400 and VLDL$_2$ S$_f$ 20–60), intermediate density (IDL S$_f$ 12–20) and low density lipoproteins (LDL S$_f$ 0–12). Normal and hyperlipemic subjects were given tracer doses of ^{131}I-labeled VLDL$_1$ and ^{125}I-labeled VLDL$_2$ and the metabolism of apoB in VLDL$_1$, VLDL$_2$, IDL, and LDL was followed over a period of 13 days. VLDL$_1$ apoB and VLDL$_2$ apoB clearance curves had an initial shoulder, a rapid decay, and a 'tail' of slowly metabolized lipoprotein. ApoB derived from VLDL$_1$ appeared in IDL over 10–50 h and exhibited bi-exponential decay that was attributed to the presence of two metabolically distinct species. A further compartment was required to explain the observation that a substantial proportion of apoB from VLDL$_2$ appeared and disappeared from the IDL density range faster than apoB derived from VLDL$_1$ delipidation. Both of the more rapidly removed IDL species gave rise to LDL apoB that was also modeled as a heterogeneous entity with two plasma compartments. ▮▮ The final model, which has much in common with previous versions (M. Berman et al. 1978. *J. Lipid Res.* **19:** 38–56), a multi-step delipidation pathway and slowly metabolized remnant compartments in VLDL, incorporates parallel delipidation routes in VLDL$_2$, IDL, and LDL. These parallel pathways linked kinetic heterogeneity in VLDL with that in IDL and LDL.—Packard, C. J., A. Gaw, T. Demant, and J. Shepherd. Development and application of a multicompartmental model to study very low density lipoprotein subfraction metabolism. *J. Lipid Res.* 1995. **36:** 172–187.

Supplementary key words kinetics • SAAM • VLDL$_1$ • VLDL$_2$ • IDL • LDL

Apolipoprotein B-100-containing very low, intermediate, and low density lipoproteins (VLDL, IDL, LDL) mediate the transport of cholesterol and triglyceride through plasma. They form part of a complex metabolic pathway whose operation is regulated by intra- and extracellular enzymes, cell membrane receptors, and transfer proteins. Kinetic studies on the apoB transport system carried out over a number of years have yielded valuable information on the causes of hypo- and hyperlipidemia and on the mechanism of action of diets and drugs. Early investigations used relatively simple methods of deriving kinetic data from radioactivity decay curves. Recently, however, multicompartmental modeling has been applied to extract maximum information from the increasingly elaborate experiments that have been performed and to deal with the recognized complexity of the system.

The first models (1–3) possessed most of the elements that are present in current versions, e.g., transfer of apoB from VLDL to LDL through a delipidation chain, multiple synthetic inputs, and slowly decaying remnant compartments. Refinements of these have facilitated the interpretation of experiments based on trace-labeled (radioiodinated) apolipoproteins, radioactive or stable isotope-labeled amino acids and lipid precursors. Several closely related versions of a VLDL-IDL-LDL model are now present in the literature and these have been applied to a large number of subjects in a variety of situations (3–8). Each seeks to define as accurately as possible all the features found in the radioactivity (or stable isotope) curves. However, these are a function of the methodology used to generate them and recent recognition that all of the lipoprotein classes under study are structurally and metabolically heterogeneous requires that the separation techniques used are taken into account when evaluating the results of modeling.

Abbreviations: VLDL, very low density lipoproteins; IDL, intermediate density lipoproteins; LDL, low density lipoproteins; HDL, high density lipoproteins; SAAM, Simulation Analysis and Modeling computer program; TMU, tetramethylurea; FCR, fractional catabolic rate; U(I), input into compartment I; L(I,J), rate constant for transfer from J to I; R(I,J), flux or transport in mg/time from J to I; IC(I), initial conditions of I; FTR, fractional transfer rate.

[1]To whom correspondence should be addressed.

Cumulative flotation ultracentrifugation is a method devised by Lindgren, Jensen, and Hatch (9) as a means of efficiently isolating fractions of defined flotation rate. It has been used extensively to separate VLDL subfractions and when these are trace labeled and their kinetics are followed (6, 10–12) it is clear that their individual metabolic properties differ. Over a number of years we have developed a multicompartmental model to describe the kinetics of lipoproteins prepared in this way. It, in common with other recently developed models (5), incorporates parallel delipidation pathways and kinetic heterogeneity into the precursor VLDL and the product lipoproteins, IDL and LDL.

METHODS

Turnover protocol

The protocol was designed to permit the study of apoB kinetics in $VLDL_1$ (S_f 60–400), $VLDL_2$ (S_f 20–60), IDL (S_f 12–20), and LDL (S_f 0–12) by trace labeling the two VLDL fractions and following the transfer of radioactivity through to products.

The methods used to prepare the $VLDL_1$ and $VLDL_2$ tracers have been described in detail elsewhere (13). Briefly, 250 ml of plasma was obtained by plasmapheresis from subjects who had fasted overnight (14 h) and the subfractions were isolated by cumulative gradient ultracentrifugation. These were labeled with $Na[^{131}I]$ and $Na[^{125}I]$, respectively, by a modification of the iodine monochloride method (14) and sterilized immediately before reinjection by filtration through a 0.45-μm filter (Acrodisc, Gelman Sciences). On the first day of the turnover (3 days after plasma donation) subjects were admitted at 8:00 AM, having fasted overnight, and an indwelling cannula was placed in a peripheral vein to facilitate repeated blood sampling. Autologous ^{131}I-labeled $VLDL_1$ and ^{125}I-labeled $VLDL_2$ were administered in rapid sequence into a peripheral vein in the opposite arm. Venous blood samples (10 ml) were collected from the cannula at 10 min, 30 min, and 1.0, 1.5, 2, 3, 4, 6, 8, 10, 14, and 24 h post-injection and daily thereafter. To minimize chylomicron production, the subjects remained fasting for the first 10 h of the study but were allowed unlimited non-caloric fluids. From 2.0-ml aliquots of plasma, apoB-containing lipoproteins $VLDL_1$, $VLDL_2$, IDL, and LDL were isolated by a modification (13) of the cumulative gradient ultracentrifugation procedure of Lindgren et al. (9). ApoB was precipitated by the addition of an equal volume of redistilled 1,1,3,3-tetramethylurea (TMU) at 37°C to each lipoprotein fraction (15) and its specific activity was determined by radioactivity counting and protein assay (13).

The mass of apoB associated with each of the four apoB-containing lipoprotein fractions was determined by replicate analyses at four times throughout the study.

$VLDL_1$, $VLDL_2$, IDL, and LDL were isolated and their total protein and TMU soluble contents were determined (15, 16) and expressed in mg/100 ml plasma. This provided apoB concentrations (total minus TMU-soluble protein) which were then corrected for centrifugal losses by a factor that was calculated by comparing the recovered $VLDL_1$ + $VLDL_2$ + IDL + LDL cholesterol to the "non-HDL" cholesterol in plasma assayed by the Lipid Research Clinic's methodology (17) on three occasions over the turnover period. Pool sizes for apoB in the four lipoprotein fractions were then taken as the product of plasma volume (4% of body weight) and the corrected plasma concentration of apoB in each fraction.

The radioactivity present in apoB in the four lipoprotein fractions at each time point was calculated as the product of the specific activity and apoB pool size. These data were then expressed as a fraction of the total apoB ($VLDL_1$ + $VLDL_2$ + IDL + LDL) radioactivity present in the 10-min sample. Model development and the derivation of kinetic constants ($L(I,J)$ where J is the source and I the destination), compartmental masses ($M(I)$), fluxes ($R(I,J)$), and inputs ($U(I)$) were performed using the SAAM30 program (18) in its interactive version. The Simulation Analysis and Modeling (SAAM) program written by Berman and Weiss (18) is a powerful tool in multicompartmental modeling and has been used extensively in the study of lipoprotein kinetics. Given an observed data set and initial estimates, the program will alter the kinetic parameters in an iterative manner until a minimum sum of squares is reached for the residual differences between observed and calculated data sets. The program requires that observed data be given an associated error of determination in order to estimate a weighting for the sum of squares of observed minus calculated differences. We adopted a fractional standard deviation of 5% for all data sets.

Thyroidal uptake of radioiodide was blocked by the oral administration of potassium iodate (170 mg twice daily). This regimen was commenced 3 days prior to injection and continued for the next 28 days. Turnovers were conducted on an out-patient basis and all subjects were instructed to adhere strictly to their established lipid-lowering diet and lifestyle.

MODEL DEVELOPMENT

Turnovers yielded seven decay curves (^{131}I-labeled apoB in $VLDL_1$, $VLDL_2$, IDL, LDL and ^{125}I-labeled apoB in $VLDL_2$, IDL, and LDL) and four measured apoB pool sizes ($VLDL_1$, $VLDL_2$, IDL, LDL) that were combined together in the SAAM analysis to generate kinetic data. The complexity of the final model was required to accommodate the features in the decay curves and to fit the measured masses to within 15%. In the description of the model that follows (Figs. 1–10) example curves are

provided for a normal subject (N1 in reference 11) and a patient with hypothyroidism (patient 1 in reference 19) who exhibited virtually all of the features required to be accommodated in the final model.

Kinetics of ^{131}I-labeled VLDL$_1$ apoB

After injection of ^{131}I-labeled VLDL$_1$, apoB disappearance from this density interval was usually rapid (**Fig. 1**) and in nearly all normotriglyceridemic subjects could be modeled as a single compartment, i.e., a single exponential function (6, 11). A 'tail' or slowly decaying component was seen in several situations, most notably that of type III hyperlipoproteinemia (20) and hypothyroidism (19, Fig. 1) and was accounted for by the addition of a slowly decaying component (compartment 12 in model 1B, Fig. 1). In subjects with moderately or severely elevated plasma triglyceride levels, the VLDL$_1$ apoB pool was increased and the disappearance curve exhibited a small shoulder before rapid decay was established. This behavior has been consistently observed by others and has been modeled by delipidation chains of varying length (2–4). In our subjects, the addition of a second 'in-line'
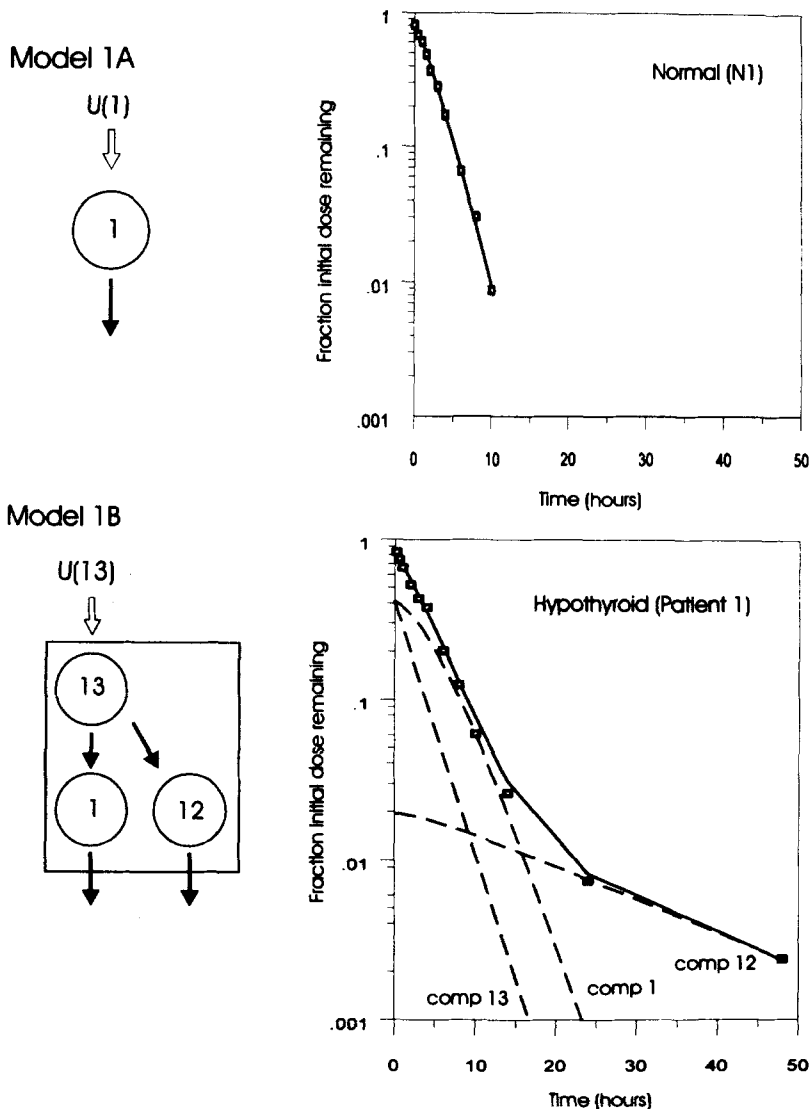

Fig. 1. Metabolism of apoB in ^{131}I-labeled VLDL$_1$. This and subsequent figures depict the metabolism of apoB in two subjects. The first is a normolipemic male (subject N1 in ref. 11) with a body weight of 71 kg, plasma cholesterol of 192 mg/dl, and plasma triglyceride of 151 mg/dl; the second, a hypothyroid female (patient 1 in ref. 19) with a body weight of 89 kg, plasma cholesterol of 495 mg/dl, and plasma triglyceride of 246 mg/dl. The hypothyroid patient was chosen as someone who exhibited most of the principal features required to be accommodated in the final model. The squares are the observed apoB radioactivities expressed as a fraction of the initial radioactivity in VLDL$_1$ + VLDL$_2$ + IDL + LDL. The solid lines are calculated (sum of compartments 1, 12, and 13) fits for VLDL$_1$ apoB using model 1B, while the dashed lines represent individual compartments. Model 1A produced acceptable fits for most normotriglyceridemic subjects (e.g., N1) but was not universally applicable.

compartment (compartment 13 in model 1B, Fig. 1) provided a satisfactory solution. The final model had a single input (U(13) into compartment 13)) and was similar to that of Berman et al. (2) and Beltz et al. (4) for the total VLDL (d < 1.006 g/ml) fraction.

Radioactivity in the tracer at time zero was distributed among the compartments according to their calculated mass. An estimate was made (usually 0.5) of the initial fraction present in compartment 13 (IC(13)) and then the initial conditions of ^{131}I-labeled VLDL apoB present in compartments 1 and 12 were calculated from the steady state equations (after the method described by Foster et al. (21)).

$$IC(1) = \frac{IC(13) \times L(1,13)}{L(0, 1) + L(2,1)}$$

$$\text{and} \quad IC(12) = \frac{IC(13) \times L(12,13)}{L(0, 12)}$$

IC(13) was allowed to change by setting it equal to an adjustable parameter (P(1) in SAAM nomenclature) as the SAAM program does not permit direct adjustment of initial conditions. Iteration of IC(13) and the intercompartmental transfer rates continued until the best curve fit was obtained. ApoB mass was distributed among compartments according to the final estimate of IC(13) and the derived values for IC(1) and IC(12). In some subjects, where there was no discernible tail to the VLDL$_1$ apoB curve, L(12,13) was set to zero (subject N1, Fig. 1; Table 1). In others, the tail was discernible but not well defined and in these cases a value for L(0,12) was estimated from the slope of the tail. L(12,13) was then derived from this slope and the intercept of the tail extrapolated back to zero time (Fig. 1). Assuming that the latter equalled IC(12) the equation above was rearranged to yield:

$$L(12, 13) = \frac{IC(12) \times L(0.12)}{IC(13)}$$

This generated an appropriate value for L(12,13) once the other parameters (P(1), L(0,1), L(2,1), L(1,13)) had been adjusted to provide a fit for the whole VLDL$_1$ apoB curve.

Kinetics of ^{131}I-labeled VLDL$_2$ apoB

A variable amount (usually 30 to 70%) of ^{131}I-labeled apoB, originally present in VLDL$_1$, appeared in the VLDL$_2$ fraction over the period of 5–15 h (**Fig. 2**). This transfer was associated with the decay of the rapid component (compartments 13 and 1) and so compartment 1 was permitted either to input radioactivity to compartment 2 in VLDL$_2$ (L(2,1), Fig. 2) or be catabolized directly from plasma, i.e., without re-entering the apoB system (L(0,1)).

The final version of the subsystem for VLDL$_2$ apoB derived from VLDL$_1$ (model 2C) is a replica of subsystem model 1B in Fig. 1. Disappearance of ^{131}I-labeled apoB from this density interval was rapid at first and then less steep with a tail indicating the presence of slowly metabolized species. The broadness of the peak was modeled by the delipidation chain of compartments 2 and 4 while compartment 6 represented a remnant population of variable abundance. As for VLDL$_1$, subjects who were hyperlipidemic tended to have high VLDL$_2$ apoB levels and a broad peak. The tail in the ^{131}I-labeled VLDL$_2$ apoB curve was again most pronounced in individuals with hypothyroidism (Fig. 2), type III hyperlipoproteinemia (20) or apoE$_2$ homozygosity (22).

Kinetics of ^{131}I-labeled IDL apoB

Radioactive apoB present in the injected ^{131}I-labeled VLDL$_1$ tracer reached IDL with a peak at 12–50 h. Subsequent disappearance from this fraction was slow and appeared to be bi-exponential in most subjects (**Fig. 3**). This feature could arise either from intra-extravascular exchange (model 3A) or from the production of two metabolically distinct IDL species from VLDL$_2$ (model 3B). The latter explanation was considered more likely for the following reasons. 1) IDL because of its size hardly penetrates the extravascular space; and 2) the relative proportions of the two exponentials (represented by compartments 8 and 9) was highly variable between subjects (the calculated ratio for M(8)/M(9) varying from 260:5 in an E$_{4/4}$ subject (patient 10 in reference 22) to 10:75 in an E$_{2/2}$ (patient 1 in reference 22) suggesting that it was not due to a physical process such as capillary permeation. Furthermore, LDL apoB was derived from the disappearance of the rapid exponential (compartment 8) indicating that this decay was due to a metabolic rather than a dilutional step.

Not all apoB leaving compartment 4 appeared in IDL compartments 8 and 9, therefore, L(0,4) was included to permit direct VLDL$_2$ catabolism. The abundance of slower metabolized IDL species in compartment 9 was determined by the tail of the ^{131}I-labeled IDL apoB curve while the more rapidly turning over IDL was modeled in compartment 8 (Fig. 3). ApoB leaving compartment 9 was lost by catabolism from the plasma (L(0,9)) as was the material in compartment 8 that did not appear in LDL (L(0,8), **Fig. 4**).

Kinetics of ^{131}I-labeled LDL apoB

The LDL decay curve observed when radioiodinated LDL is injected as tracer is bi-exponential and, traditionally, modeled as a single plasma compartment equilibrating with extravascular space (23) in line with the general analysis formulated for plasma proteins (24). However, when urinary radioactivity excretion data are taken into
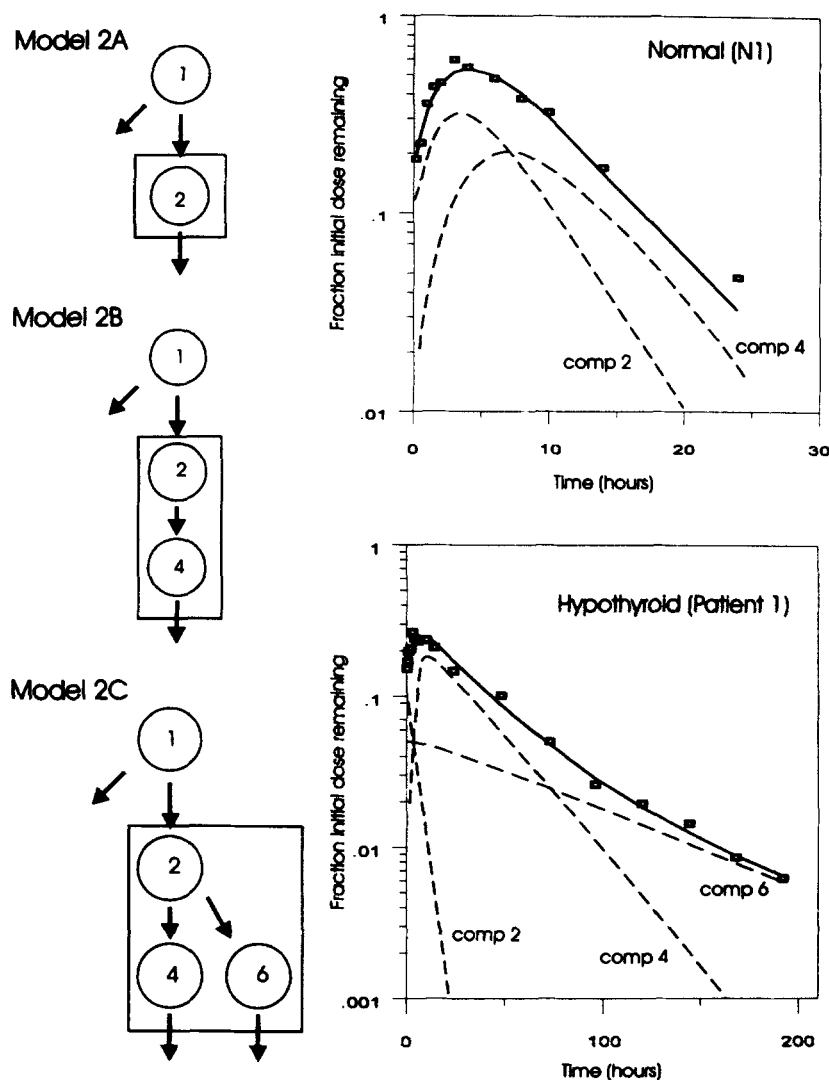
Fig. 2. Metabolism of ^{131}I-labeled apoB in VLDL$_2$. Subsystem model 2C was applied to the data for VLDL$_2$ ^{131}I-labeled apoB radioactivity to generate the fitted curves. The solid lines are the sum of compartments 2, 4, and 6 while the dashed lines show their individual decays. Models 2A and 2B were too simple to produce satisfactory fits.

account, the situation becomes more complex in that the daily urine/plasma radioactivity ratio, which should be constant with time according to Matthews (24), declines during the turnover period. To accommodate this finding a second, more rapidly metabolized plasma compartment is added (21, 25, 26) so that unlike the situation for other, homogeneous plasma proteins (e.g., albumin) the early rapid decay for LDL is a combination of catabolism and dilution into the extravascular space. Recently published LDL turnovers (21, 26) analyzed by a two plasma compartment model now predict much less extravascular penetration of the tracer (in our studies (26) about 10–15% compared to 25% in the classical Matthews analysis).

ApoB appearing in the LDL density interval following delipidation of the ^{131}I-labeled VLDL$_1$ tracer exhibited two principal features (Fig. 4). First, in many subjects a

substantial period of time elapsed before peak radioactivity was observed (up to 5 days in patients with hypothyroidism (Fig. 4) or homozygous familial hypercholesterolemia (FH(11)). Second, the decay appeared mono-exponential in virtually all subjects (Fig. 4) regardless of whether the peak occurred early or late.

The standard Model 4A (Fig. 4) was applied to LDL decay curves but this usually resulted in poorly defined intra-extravascular transfer rates which often reverted to zero or a very low value upon iteration. If this occurred then an LDL subsystem with a single plasma compartment (model 4B) was adopted for the subject and this produced satisfactory fits as seen in Fig. 4. In the few subjects where ^{131}I-labeled LDL apoB decay was clearly bi-exponential model 4A was retained. Undoubtedly extravascular equilibration occurs in all subjects as LDL is
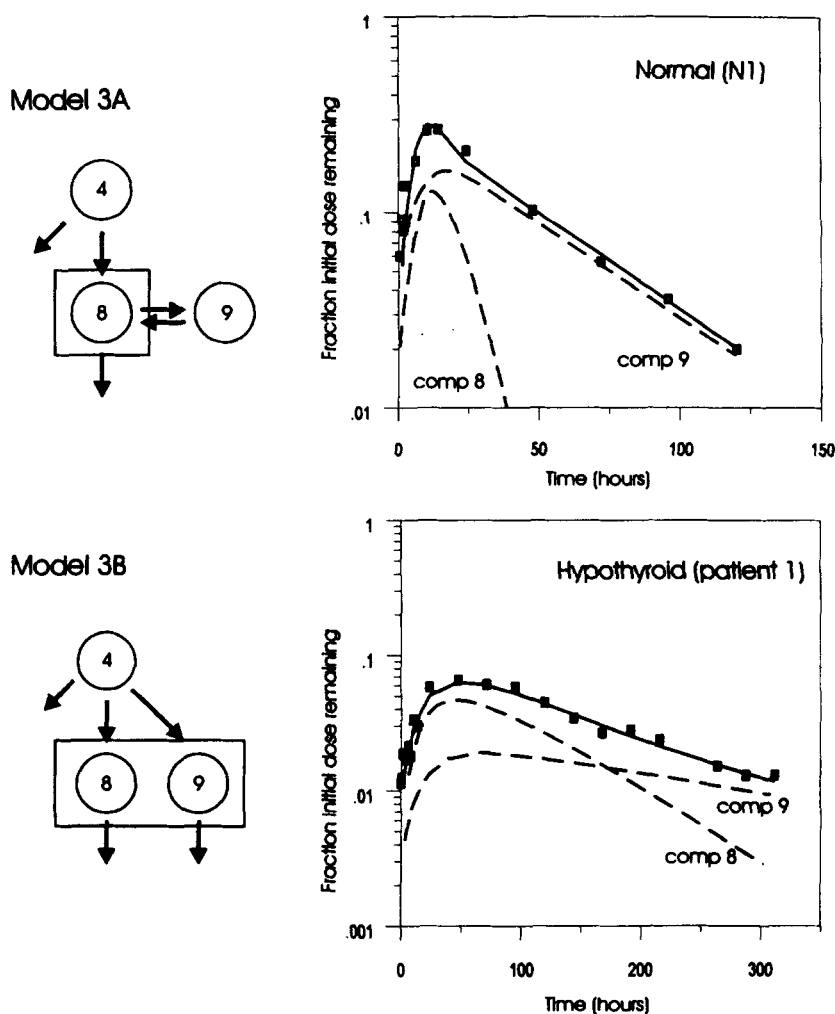
Fig. 3. Metabolism of ^{131}I-labeled apoB in IDL. Subsystem model 3B was applied to the IDL radioactivity data (squares) to generate the fitted curves. The solid lines are the sum of compartments 8 and 9. Model 3A which included an extravascular IDL compartment failed to provide a satisfactory fit to the mass of IDL and required capillary transfer rates to vary over an unacceptably wide range.

found in interstitial fluid (27) but there was insufficient information in the decay curves to permit its quantitation. For example, in simulations where ^{131}I-labeled apoB in LDL was forced to exchange with compartment 14, little difference could be seen in the appearance and disappearance curves (Fig. 4) until the extravascular LDL compartment exceeded 10% of the body pool.

In a few subjects the fit of ^{131}I-labeled apoB radioactivity in LDL and the agreement between observed and expected LDL apoB mass was improved by a bypass route from compartments 4 to 11 (L(11,4)) (e.g., Table V in ref. (22). This was incorporated in the final ^{131}I-labeled VLDL$_1$ tracer model as shown in **Fig. 5.**

Metabolism of ^{125}I-labeled VLDL$_2$

As tracers of both VLDL$_1$ and VLDL$_2$ were administered simultaneously, the final compartmental model had to predict for the VLDL$_2$ density interval and for the products IDL and LDL the behavior of apoB from both sources (^{125}I and ^{131}I). In constructing a model for ^{125}I-labeled VLDL$_2$ we attempted first to adopt the ^{131}I-labeled VLDL$_1$ apoB system (model 5 in Fig. 5) and distributed ^{125}I-labeled VLDL$_2$ tracer within the VLDL$_2$ density range in proportion to the masses calculated for compartments 2, 4, and 6 with no input at the VLDL$_2$ level (i.e., U(13) was the only source of VLDL apoB production in analogy with the early model of Berman et al. (2)). This maneuver did not produce a satisfactory fit to either the decay curves or the masses of VLDL$_2$, IDL, or LDL. There was a substantial shortfall in the predicted mass in all three density intervals indicating that input of apoB was required at the level of VLDL$_2$. Thus, in a second model, we permitted VLDL apoB input into compartment 2 (U(2) in model 6, Fig. 5)). This improved the agreement between calculated and observed masses but did not produce a good fit for the ^{125}I-labeled apoB decay
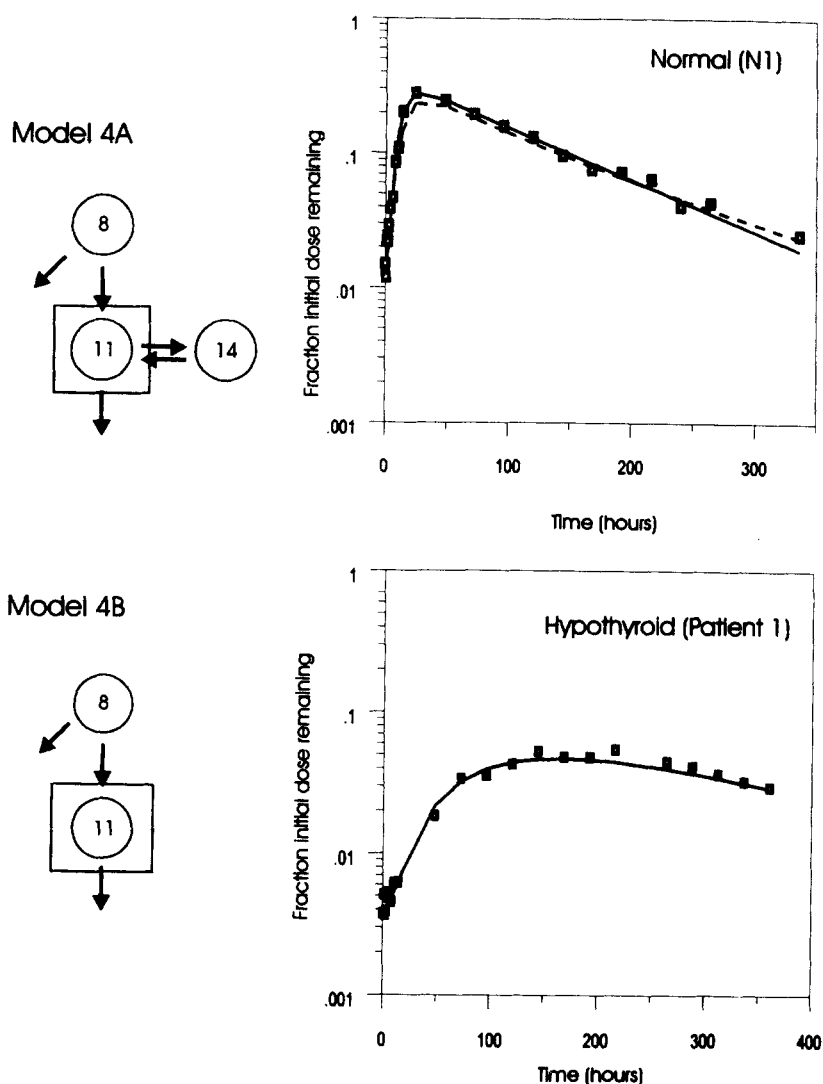
Fig. 4. Metabolism of ^{131}I-labeled apoB in LDL. Subsystem models 4A and 4B were applied to the data sets. Inclusion of an extravascular exchange compartment (compartment 14) did not improve the fit and thus model 4B was used for these two and most other subjects. An example of the impact of extravascular exchange is provided for subject N1. The dashed line was the result of a simulation in which an extravascular compartment accounted for 12% of whole body LDL.

curves in $VLDL_2$, IDL, or LDL (**Fig. 6**). An extra, early and rapid decay was present in the ^{125}I-labeled $VLDL_2$ apoB curve and in IDL and LDL a substantial component of radioactive apoB appeared and disappeared more quickly than model 6 predicted. These observations indicated that the metabolic characteristics of the ^{125}I-labeled $VLDL_2$ tracer could not be explained simply by its insertion later in the delipidation cascade and indicated that apoB appearing for the first time in the $VLDL_2$ density interval had a kinetic behavior that was distinct from that derived from large, triglyceride-rich $VLDL_1$, i.e., parallel delipidation channels were required. The concept of metabolic channels within the VLDL-IDL-LDL delipidation cascade was first mooted by Fisher (28) and incorporated in recent models (5). The introduction of this feature into the combined ^{131}I-labeled $VLDL_1$ apoB, ^{125}I-labeled $VLDL_2$ apoB model permitted resolution of the discrepancies noted above and provided satisfactory fits to both radioactivity curves and apoB masses in all fractions.

Kinetics of ^{125}I-labeled $VLDL_2$ apoB

The simplest addition to the $VLDL_2$ subsystem in Fig. 5 that permitted input of apoB and the potential for rapid catabolism was the inclusion of a fourth compartment not linked to others (**Fig. 7**, model 7). Thus, the final model for ^{125}I-labeled $VLDL_2$-apoB comprised this compartment (compartment 5) and a system of compartments whose kinetics were dictated by the behavior of ^{131}I-labeled apoB derived from the $VLDL_1$ tracer. In the
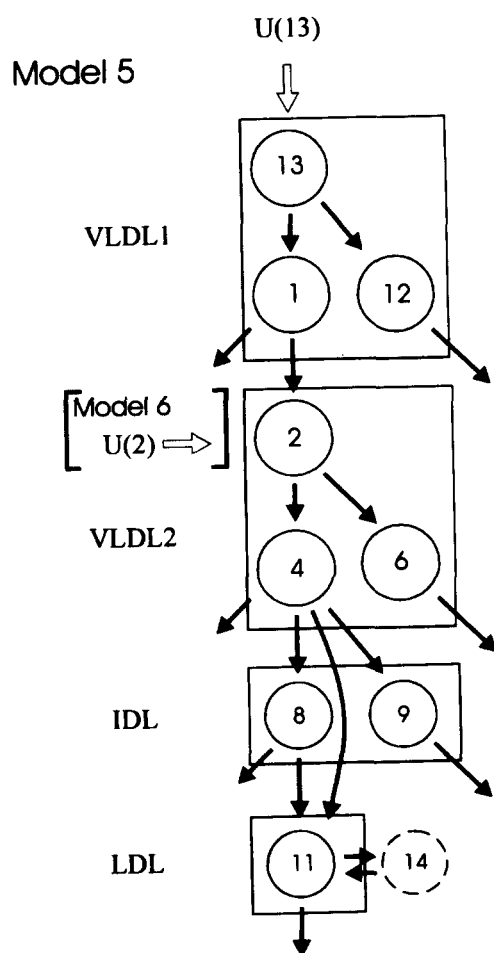
Fig. 5. The composite model for VLDL$_1$ apoB metabolism contained a VLDL delipidation chain (compartments 13, 1, 2, 4) and 'remnant' populations (compartments 12 and 6). The model is highly analogous to that originally described by Berman et al. (2). Model 6, which comprised model 5 with additional input at the level of compartment 2, was used to fit the ^{125}I-labeled VLDL$_2$ apoB decay curves. As seen in Fig. 6 this was unsatisfactory.

SAAM model specification this was achieved by setting *the rate constants equal to those of Fig. 2, model 2C*, i.e., L(26,22) = L(6,2), L(24,22) = L(4,2), L(0,24) = L(0,4) etc. Compartment 5 had its own input (U(5)) and elimination constant. As for ^{131}I-labeled VLDL$_1$ apoB tracer, the initial conditions (i.e., time zero radioactivities) for ^{125}I-labeled VLDL$_2$ apoB had to be distributed over the compartments. For the ^{125}I-labeled VLDL$_2$ tracer this was achieved by the use of two adjustable parameters, P(2) and P(3). P(2) was the total ^{125}I-labeled apoB radioactivity present in the VLDL$_2$ density interval at time zero (theoretically 100%) while P(3) was an estimate of the fraction of this present in compartment 22. Initial conditions were derived for compartments 24 and 26 by the equations:

$$IC(22) = P(3)$$

$$IC(24) = \frac{L(24,22) \times P(3)}{L(I,24)}$$

$$\text{and} \quad IC(26) = \frac{L(26,22) \times P(3)}{L(0,26)}$$

(L(I,24) equals the sum of all rate-constants leaving compartment 24) which state that the distribution of radioactivity in the VLDL$_2$ tracer is proportional to the compartmental masses. The initial condition of compartment 5 was then calculated as:

$$IC(5) = P(2) - P(3) - IC(24) - IC(26).$$

In subjects studied to date, IC(5) ranged from 10% to 70% of the total VLDL$_2$ radioactivity. U(22) is included in the model to provide input to that part of the model which reflects apoB derived from VLDL$_1$. The mass of compartment 22 was set equal to that of compartment 2 and since the rate constants L(24,22) and L(26,22) are dependent as noted above, U(22) by definition equals the flux of apoB from compartments 1 to 2 in model 5 and as such is a dummy variable required by the SAAM program to generate steady state masses in the ^{125}I-labeled VLDL$_2$ model. The masses of compartments 24 and 26 were derived from the final values of IC(24) and IC(26). The mass in compartment 5 was calculated from the equation:

$$M(5) = IC(5) \times \frac{M(22)}{IC(22)}$$

which assigns a mass in proportion to the final estimate for the initial conditions. This relationship provides for a constant starting specific activity in all compartments that comprise the ^{125}I-labeled VLDL$_2$ tracer.

Application of model 7 to the ^{125}I-labeled VLDL$_2$ apoB curves provided a satisfactory fit to observed data (Fig. 7). The ^{131}I-labeled apoB-defined subsystem explained the later part of the VLDL$_2$ curve while compartment 5 correctly predicted the early, rapid clearance. Connecting compartment 5 to compartments 24 or 26 did not improve the fit.

Kinetics of ^{125}I-labeled IDL apoB

Addition of a single, independent compartment (compartment 7) to an IDL subsystem (compartments 28 and 29) whose kinetics were dictated by compartments 8 and 9 in model 5 (**Fig. 8,** model 8) led to the generation of acceptable fits for both the ^{125}I-labeled apoB radioactivity curve and the observed mass. In most subjects virtually all
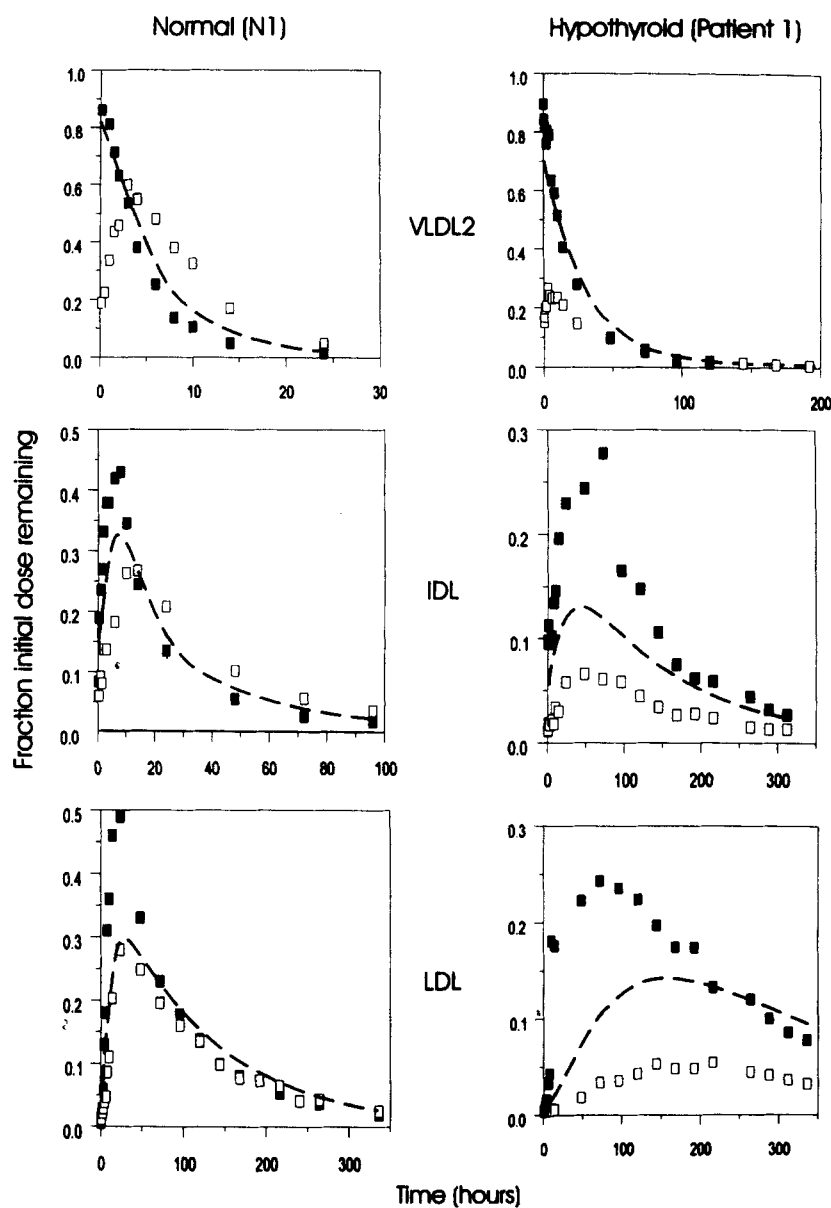
Fig. 6. Metabolic properties of ^{131}I-labeled $VLDL_1$ apoB and ^{125}I-labeled $VLDL_2$ apoB in a normal and hypothyroid patient. The open squares are ^{131}I-labeled apoB radioactivity and the filled squares are ^{125}I-labeled apoB. Linear scales were chosen in order to see more clearly the inability of model 6 to explain the ^{125}I-labeled apoB data. The predicted curves (dashed lines) from model 6 tended to fit the later components in each curve. However, in both IDL and LDL ^{125}I-labeled apoB there was a substantial component that appeared and disappeared rapidly.

of the apoB radioactivity ascribed to compartment 5 (Fig. 7) appeared rapidly in compartment 7 (Fig. 8) with little being lost by direct catabolism (L(0,5)). This, in turn, decayed quickly and was transferred into the LDL density range. Again, there was no requirement for a connection between compartment 7 and other IDL compartments. Therefore, the delipidation chain of compartments 5 and 7 represented a parallel, independent pathway. The IDL apoB mass predicted by model 8 was close to that observed in the vast majority of subjects across a wide range

of physiological and pathological conditions. Hence, there was no requirement for direct input of apoB into IDL.

Kinetics of ^{125}I-labeled LDL apoB

The kinetic behavior of ^{125}I-labeled LDL apoB derived from $VLDL_2$ was explained by the presence of two plasma compartments, one (compartment 31) whose metabolism was tied to that of compartment 11 in model 5 and a second which represented the terminal stage of delipidation of apoB originally in compartment 5 in $VLDL_2$ (Fig. 7).
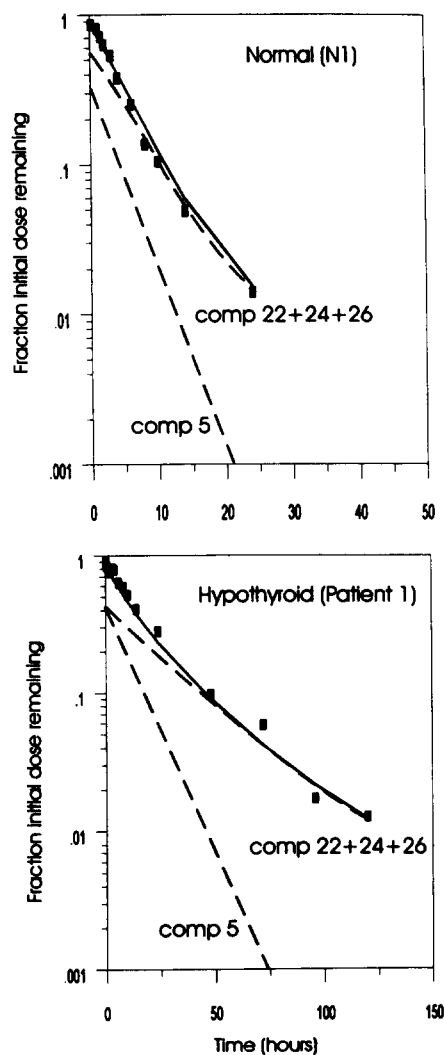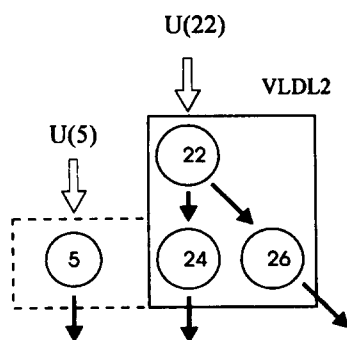
Model 7

U(5)

U(22)

VLDL2

22

5

24

26

Normal (N1)

comp 22+24+26

comp 5

Fraction initial dose remaining

Hypothyroid (Patient 1)

comp 22+24+26

comp 5

Time (hours)

Fig. 7. Metabolism of ^{125}I-labeled apoB in the VLDL$_2$. When an additional compartment 5 was added to the VLDL$_2$ subsystem in model 5, satisfactory fits (solid lines, the sum of compartments 5, 22, 24, and 26) were obtained to the observed data (squares). Compartments 22, 24, and 26 were used to permit a portion of ^{125}I-labeled apoB radioactivity to mirror compartments 2, 4, and 6 for ^{131}I-labeled apoB radioactivity. This was achieved by setting L(24,22), L(26,22), L(0,24), and L(0,26) equal to L(4,2), L(6,2), L(0,4), and L(0,6), respectively. U(22) was used to permit steady state calculation of total VLDL$_2$ mass. It is equivalent to the flux of apoB from compartment 1 to 2 in model 5. U(5) provided input into the independent compartment 5. The contributions of compartment 5 versus the subsystem dictated by ^{131}I-labeled apoB kinetics (compartments 22 + 24 + 26) are shown by the dashed lines.

The apoB in compartment 10 appeared and then decayed more rapidly than that in compartment 31 (**Fig. 9**). Implicit in the subsystem model (model 9B, Fig. 9) was the concept that LDL was metabolically heterogeneous and the bi-exponential nature of ^{125}I-labeled apoB decay in the LDL density interval was primarily the result of this phenomenon rather than intra-extravascular exchange. A two plasma compartment model for LDL apoB is in line with current concepts of the metabolism of this lipoprotein class in normal and dyslipidemic subjects (21, 25, 26, 29). For subjects who required an extravascular compartment in the ^{131}I-labeled apoB subsystem, model 9A was adopted for ^{131}I-labeled LDL apoB.

The mass of LDL apoB predicted to arise from the delipidation of VLDL$_1$ was usually substantially less than that observed. In the hypothyroid subject whose data are shown in Figs. 1–4, delipidation of VLDL$_1$ apoB generated a peak of only 5% in apoB radioactivity in LDL. The steady state LDL apoB mass calculated to result from this transfer was 576 mg compared to a total observed mass of 3668 mg (19). VLDL$_2$ delipidation, on the other hand, led to a peak value of 25% in ^{125}I-labeled LDL apoB (Figs. 6 and 9) indicating that transfer down the 5 → 7 → 10 chain was not only rapid but more complete. This pathway provided a further 2215 mg of LDL apoB. However, even when the flux from both VLDL$_1$ and
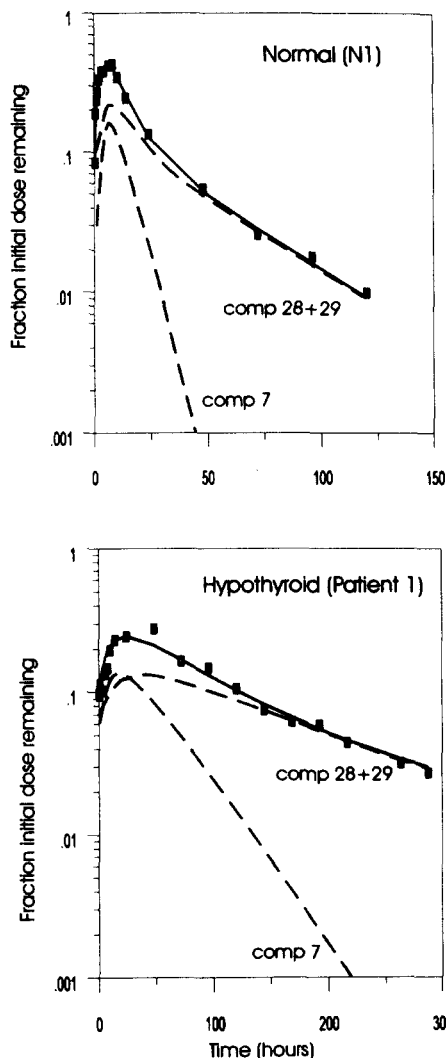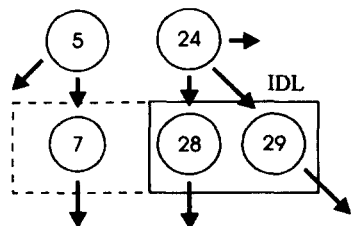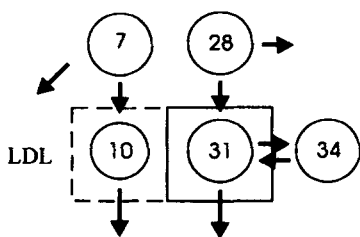
Model 8

Fig. 8. Metabolism of ^{125}I-labeled apoB in IDL. Compartments 28 and 29 were defined by setting L(0,24), L(28,24), L(29,24), L(0,28), L(31,28), and L(0,29) equal to L(0,4), L(8,4), L(9,4), L(0,8), L(11,8), and L(0,9), respectively. Compartment 5 in the VLDL$_2$ subsystem fed compartment 7 and also was catabolized directly. The solid line is the sum of compartments 7, 28, and 29. Dashed lines are shown for the components explained by ^{131}I-labeled apoB kinetics (compartments 28 and 29) and the additional compartment 7 needed to fit the observed data (solid squares).

VLDL$_2$ was taken into account, there was still a substantial difference between predicted and observed LDL masses in this patient and in a large number of other subjects (30) and so further input was required. Other workers have observed this phenomenon and introduced rapid metabolism pathways from newly secreted VLDL into LDL to help explain it (4). However, when we attempted similar maneuvers — the addition of the compartment 5 → 10 and 4 → 11 rapid delipidation routes — to eliminate this shortfall, it was diminished but not abolished. Further, the inclusion of a rapid transfer from compartment 1 to compartment 11 was also unhelpful as, in most instances, the rate of rise in apoB radioactivity in compartment 11 (Figs. 4, 6) was slow; e.g., in the

hypothyroid patient, 15 h after injection, 97% of apoB radioactivity had disappeared from the VLDL$_1$ density interval but only a minor fraction (1%) had transferred to LDL (Fig. 4). As an alternative, direct LDL input was invoked to make up the discrepancy between observed and calculated mass. As it could not be known whether input was into compartment 10 or 11, the input rate was calculated as the product of the shortfall in mass and the overall LDL FCR i.e.,

$$\text{Direct input} = \frac{\text{Unexplained}}{\text{LDL apoB mass}} \times \frac{R(0,11) + R(0,10)}{M(10) + M(11)}.$$
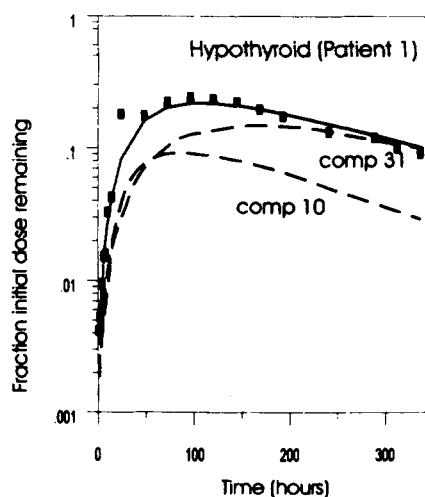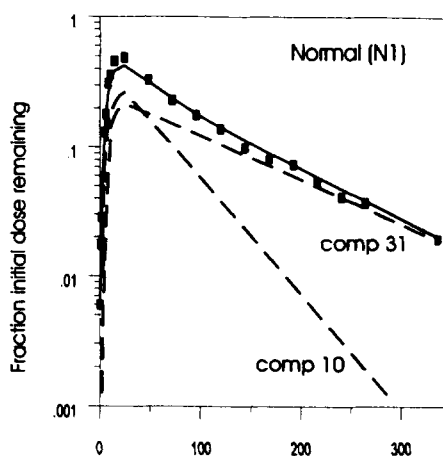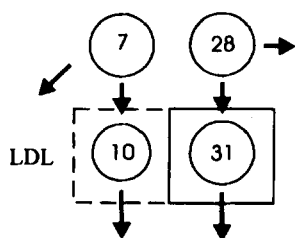
Model 9A

Model 9B

Fig. 9. Metabolism of ^{125}I-labeled apoB in LDL. Compartment 31 was defined by setting L(0,28), L(31,28), and L(0,31) equal to L(0,8), L(11,8), and L(0,11), respectively. Of the ^{125}I-labeled apoB disappearing from IDL compartment 7 some appeared in LDL (L(10,7)) and some was catabolized directly (L(0,7)). In subjects with a clear biexponential curve in ^{131}I-labeled apoB in LDL compartment 34 was included and its kinetics were made dependent on compartment 14. The contributions of compartment 10 (derived from apoB first appearing in VLDL$_2$) and compartment 31 (reflecting LDL apoB generated from VLDL$_1$ delipidation) are shown as dashed lines. The solid lines are the calculated fit for compartments 10 plus 31.

INTEGRATED MODEL FOR VLDL$_1$ AND VLDL$_2$ apoB METABOLISM

Model 10 (**Fig. 10**) was applied to the ^{131}I-labeled and ^{125}I-labeled apoB radioactivity data and the results for the two subjects in the figures are given in **Table 1.** Further constraints on the fitting procedure were achieved by including the measured apoB masses in VLDL$_1$, VLDL$_2$, IDL, and LDL as observed compartments using the G function in SAAM, e.g.,

$$G(4) = M(10) + M(31).$$

Parameter adjustment was performed using all three data sets (^{131}I, ^{125}I and masses) simultaneously and, fol-

lowing iteration, the estimates in Table 1 were obtained. Fractional standard deviations generated for the individual rate constants were typically in the range 5–15% for L(7,5), L(10,7), L(11,8), L(0,10), and L(0,11) and 15–50% for L(0,7), L(0,8), L(0,9), L(8,4), L(9,4), L(0,4), L(6,2), L(4,2), L(0,5), L(0,6), L(2,1), L(1,13), and L(0,1) (Table 1). The precision of the estimate in the latter group depended greatly on the extent to which the pathway was used. Less well defined, except for hypertriglyceridemics, were L(0,12) and L(13,12). The percentage and amount of direct LDL apoB input was determined by the difference between the observed versus calculated LDL apoB mass. The value obtained, therefore, included the accumulated errors associated with these measurements and must be
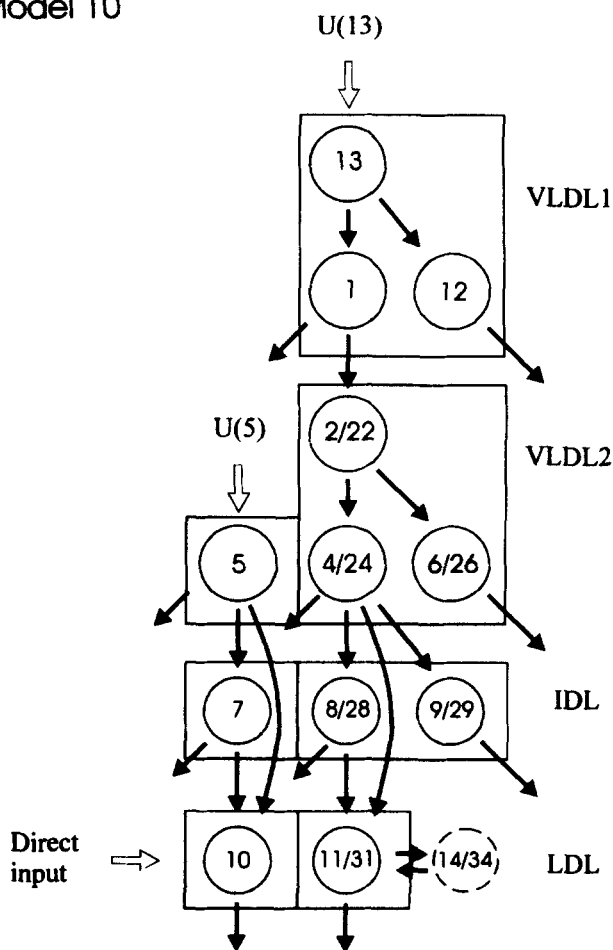
Model 10

Fig. 10. Final model of VLDL apoB metabolism. The final model developed to explain ^{131}I-labeled VLDL$_1$ and ^{125}I-labeled VLDL$_2$ apoB metabolism had to fit both sets of decay curves (Fig. 6) and the measured apoB masses in VLDL$_1$, VLDL$_2$, IDL, and LDL. In the model shown here ^{131}I-labeled apoB radioactivity decay curves were modeled by compartments 1, 2, 4, 6, 8, 9, 11–13. The ^{125}I-labeled VLDL$_2$ model had to include the kinetics of apoB derived from VLDL$_1$ as dictated by compartments 22–29, 31, and 34 and also allow for independent behavior of apoB input at the level of VLDL$_2$ in compartments 5, 7, and 10.

considered an approximation. Nevertheless, the parameter did exhibit meaningful relationships with other kinetic variables and plasma lipid and lipoprotein levels (30).

For ease of presentation and interpretation (see accompanying paper (30)), summary rates of the fraction of lipoprotein apoB (in pools/day) removed by direct catabolism and the fraction subject to delipidation were calculated for VLDL$_1$, VLDL$_2$, IDL, and LDL as follows (R(I,J)) = flux from J to I in mg/day):

A. Fraction of VLDL$_1$ apoB removed by direct catabolism =
$$\frac{R(0,1) + R(0,12)}{M(1) + M(12) + M(13)}$$

B. Fraction of VLDL$_1$ apoB transferred to VLDL$_2$ =
$$\frac{R(2,1)}{M(1) + M(12) + M(13)}$$

C. Fraction of VLDL$_2$ apoB removed by direct catabolism =
$$\frac{R(0,5) + R(0,4) + R(0,6)}{M(2) + M(4) + M(5) + M(6)}$$

D. Fraction of VLDL$_2$ apoB transferred to IDL/LDL =
$$\frac{R(8,4) + R(9,4) + R(11,4) + R(7,5) + R(10,5)}{M(2) + M(4) + M(5) + M(6)}$$

TABLE 1.

Parameter	Subject N1		Hypothyroid patient	
	Value	FSD[a]	Value	FSD
	h^{-1}		h^{-1}	
L(0,1)	0.156	0.24	0.297	0.27
L(1,13)	0.57	0.44	0.393	0.31
L(12,13)	0.0	-	0.002	[c]
L(0,12)	0.0	-	0.048	[b]
L(2,1)	0.437	0.33	0.072	0.28
L(4,2)	0.312	0.42	0.440	0.21
L(6,2)	0.0005	0.35	0.008	0.26
L(0,6)	0.009	[b]	0.011	0.02
L(0,4)	0.054	0.28	0.022	0.06
L(0,5)	0.099	0.39	0.041	0.15
L(8,4)	0.149	0.44	0.010	0.09
L(7,5)	0.195	0.11	0.043	0.06
L(10,5)	0.0	-	0.0	-
L(9,4)	0.034	0.39	0.0031	0.25
L(11,4)	0.0	-	0.0	-
P(3)[d]	0.23	0.24	0.03	0.21
L(0,7)	0.0	-	0.0	-
L(10,7)	0.116	0.09	0.026	0.06
L(0,8)	0.044	0.33	0.0	-
L(11,8)	0.102	0.10	0.013	0.10
L(0,9)	0.020	0.04	0.0036	0.11
L(0,10)	0.0168 (0.0168)[e]	0.06 (0.07)[e]	0.0055 (0.0055)[e]	0.06 (0.06)[e]
L(0,11)	0.0083 (0.0092)[e]	0.02 (0.04)[e]	0.0041 (0.0039)[e]	0.11 (0.12)[e]

[a] Fractional Standard Deviation.
[b] These parameters were estimated from the slope of the "tail" part of the curve in VLDL$_1$ or VLDL$_2$. They were fixed during iteration as there were insufficient data to permit a good definition of the rate constant.
[c] L(12,13) was a dependent rate in this patient and calculated from the equation L(12,13) $\cdot$ IC(12) $\times$ L(0,12)/IC(13) assuming that IC(12) equalled the intercept on the y axis of the tail of the VLDL$_1$ apoB curve.
[d] P(3) is the fraction of ^{125}I-labeled VLDL$_2$ apoB estimated to be present in compartment 22.
[e] The values in brackets are those obtained when an extravascular LDL compartment (compartment 14) was included to give a percent extravascular LDL of 12%. The FCR for LDL with and without such an extravascular compartment in the model was 0.32 and 0.31, respectively, for N1 and 0.125, and 0.121, respectively, for the hypothyroid patient.

E. Fraction of IDL apoB removed by direct catabolism $=$
$$\frac{R(0,7) + R(0,8) + R(0,9)}{M(7) + M(8) + M(9)}$$

F. Fraction of IDL apoB transferred to LDL $=$
$$\frac{R(10,7) + R(11,8)}{M(7) + M(8) + M(9)}$$

G. Fraction of LDL apoB removed by direct catabolism $=$
$$\frac{R(0,10) + R(0,11)}{M(10) + M(11)}$$

The overall fractional catabolic rate (FCR) for $VLDL_1$ apoB is the sum of A + B. Similarly the FCRs for $VLDL_2$ apoB and IDL apoB are equal to C + D and E + F, respectively. For LDL the FCR is equal to G. The reciprocal of the overall FCR is the Residence Time of a lipoprotein and this is presented as an index of overall clearance in the tables of the accompanying paper (30).

DISCUSSION

The model described above has a great deal in common with those developed by others, notably Berman et al. (2) and Fisher et al. (3, 28). These workers introduced the concepts of the delipidation chain to describe VLDL kinetics and metabolic channelling to account for heterogeneity in VLDL and its metabolic products. In model 10 the chain of compartments 13, 1, 2, 4 is analogous to the delipidation sequence seen in previous publications while compartments 6 and 12 represent the slowly decaying 'tail' species identified as compartment 21 by Berman et al. (2) in total VLDL. Splitting the chain between $VLDL_1$ and $VLDL_2$ and allowing internal transfer rates to vary (i.e., L(1,13) and L(4,2) in model 10) provided considerable flexibility in describing VLDL apoB metabolism. In the model of Beltz et al. (4), a similar effect was achieved for total VLDL by varying the number of compartments in the delipidation cascade rather than having four with identical fractional transfer rates as defined in the original concept (2). Our observation that a substantial portion of $VLDL_1$ apoB was directly catabolized (30) led to a further minor modification of the earlier models (2, 4) in that a removal pathway was required near the beginning of the chain (L(0,1)). However, it was our adoption of the fractionation technique of cumulative flotation ultracentrifugation (9) that dramatically increased the complexity of the model required to fit the data. We found (6) that when VLDL subfractions were used as tracers, a second parallel delipidation route to IDL and LDL, arising in $VLDL_2$, was required to fit observed masses and the differential kinetic behavior of apoB derived from $VLDL_1$ and $VLDL_2$ (Fig. 6). Fisher

et al. (5) have also recently reported, in FH patients, the presence of VLDL and LDL heterogeneity and the generation of LDL by both a VLDL delipidation chain and rapid metabolism of a VLDL sub-compartment.

It is important that compartmental models describing apoB metabolism should be applicable to normals and the extremes of hyperlipidemia. The model (model 10) has been used to describe apoB kinetics in homozygous FH on one hand (11) and lipoprotein lipase deficiency (12) on the other as well as the more subtle changes seen in normolipemic $apoE_2$ and $apoE_4$ homozygosity (22). In each case multicompartmental modeling pinpointed specific steps that were deficient or accelerated. In LpL deficiency (12) it was observed that $VLDL_1$ delipidation and catabolism was severely impaired while the metabolism of $VLDL_2$ was almost normal whereas in FH, $VLDL_1$ kinetic behavior was similar to controls while that of $VLDL_2$ was aberrant (11). The desirability of studying $VLDL_1$ and $VLDL_2$ separately was further seen in an investigation in NIDDM patients (31). When the subjects were examined in the untreated state, nearly all apoB input in VLDL was at the level of $VLDL_1$ and the radioactivity curves in $VLDL_2$, IDL, and LDL were virtually identical for both the ^{131}I-labeled $VLDL_1$ and ^{125}I-labeled $VLDL_2$ tracers. Insulin therapy specifically inhibited $VLDL_1$ apoB input and, during treatment, the apoB curves in $VLDL_2$, IDL, and LDL generated from the two tracers differed markedly in a manner similar to those shown in Fig. 6. This experience has led us to the conclusion that the kinetic heterogeneity seen in the precursors $VLDL_1$ and $VLDL_2$ is linked to that in the products IDL and LDL.

Cumulative flotation ultracentrifugation makes possible the recovery of triglyceride-rich lipoprotein subfractions of defined flotation interval such as $VLDL_1$ and $VLDL_2$. It also separates IDL from LDL in a way that differs fundamentally from the more traditional approach of fixed density centrifugation. This had an impact on the IDL and LDL apoB radioactivity curves that we observed and hence on the model and the meaning of derived kinetic parameters. In an early study (6) we compared various methods of IDL/LDL separation—centrifugation at densities 1.019 and 1.025 g/ml and cumulative flotation—and found that the clearance curve of IDL, the peak attained in LDL, and the extent to which the bi-exponential nature of LDL decay was emphasized differed substantially between them. Fixed density techniques appeared to include in LDL lipoprotein particles that were classified as IDL by cumulative flotation. The distinction between "IDL" and "LDL" at the S_f 12 boundary must be considered arbitrary as there is no distinct trough in the S_f 0–400 lipoprotein spectrum at this point. However, support for the suggestion that the cumulative flotation method provides better fractionation comes from the finding of Musliner, Giotas, and Krauss (32) that LDL (d 1.019–1.063 g/ml) prepared by conventional methodology

is "commonly contaminated with lipoproteins belonging to both the IDL_1 and IDL_2 particle distributions." Thus caution is needed when comparing IDL and LDL kinetics obtained by the fixed density methods with those obtained using cumulative flotation.

It was noteworthy that we observed, as did Beltz et al. (4) that IDL apoB decay in nearly all subjects was biexponential especially when the period of observation was extended to 200 h rather than the 48 h normally used. Unlike the earlier study (4) we found that the slowly metabolized IDL apoB component was substantial in many individuals and could not be excluded from analysis. Thus, a two plasma compartment IDL subsystem (model 10) was constructed rather than the single compartment used by others (2, 4). The need for the second IDL compartment was undoubtedly a further function of the use of cumulative flotation which provides much higher IDL apoB masses than centrifugation at d = 1.019 g/ml (4, 30). We, therefore, observed higher transport rates through IDL apoB but in some instances there was still the need to postulate transfer from $VLDL_2$ to LDL bypassing plasma IDL (L(10,5) and L(11,4)) in agreement with the earlier finding of Beltz et al. (4) in order to account for all the radioactive apoB appearing in LDL from $VLDL_2$.

LIMITATIONS OF THE MODEL

Many of the features in the model shown in Fig. 10 are, as noted above, dictated by the lipoprotein separation methodology and care should be taken when comparing the results with turnovers performed using other techniques; there is a great deal of agreement but there are also significant differences. Our approach to describing the whole of the apoB metabolic cascade was impaired by the lack of information regarding the kinetics of IDL and LDL produced from sources other than the injected VLDL tracers. We assumed that LDL generated by direct production had the same FCR as LDL formed from VLDL delipidation. Further, it was also assumed that as the predicted mass of IDL apoB was in agreement with that observed, then no direct IDL input occurred. While this may be the case in normal subjects, others are likely to exhibit direct input of apoB into this density range (5). Some of this will be converted to LDL and, hence, account for a potentially substantial fraction of LDL direct input. Despite the complexity of the model some features such as the chain of compartments 5, 7, and 10 is potentially constricting especially if subjects make mostly $VLDL_2$ and little $VLDL_1$, although we have not yet observed a situation where the model did not generate a satisfactory fit. ∎

REFERENCES

1. Phair, R. D., M. G. Hammond, J. A. Bowden, M. Fried, W. R. Fisher, and M. Berman. 1975. A preliminary model for human lipoprotein metabolism in hyperlipoproteinemia. *Fed. Proc.* **34:** 2263–2270.
2. Berman, M., M. Hall III, I. Levy, S. Eisenberg, D. W. Bilheimer, R. D. Phair, and R. H. Goebel. 1978. Metabolism of apoB and apoC lipoproteins in man: kinetic studies in normal and hyperlipoproteinemic subjects. *J. Lipid Res.* **19:** 38–56.
3. Fisher, W. R., L. A. Zech, P. Bardaleye, G. Warmke, and M. Berman. 1980. The metabolism of apolipoprotein B in subjects with hypertriglyceridemia and polydisperse LDL. *J. Lipid Res.* **21:** 760–774.
4. Beltz, W. F., Y. A. Kesaniemi, B. V. Howard, and S. M. Grundy. 1985. Development of an integrated model for analysis of the kinetics of apolipoprotein B in plasma very low density lipoproteins, intermediate density lipoproteins and low density lipoproteins. *J. Clin. Invest.* **76:** 575–585.
5. Fisher, W. R., L. A. Zech, L. L. Kilgore, and P. W. Stacpoole. 1991. Metabolic pathways of apolipoprotein B in heterozygous familial hypercholesterolemia: studies with a [³H]leucine tracer. *J. Lipid Res.* **32:** 1823–1836.
6. Packard, C. J., A. Munro, A. R. Lorimer, A. M. Gotto, and J. Shepherd. 1984. Metabolism of apolipoprotein B in large triglyceride-rich very low density lipoproteins of normal and hypertriglyceridemic subjects. *J. Clin. Invest.* **74:** 2178–2192.
7. Ginsberg, H. N., N-A. Le, and J. L. Gibson. 1985. Regulation of the production and catabolism of plasma low density lipoproteins in hypertriglyceridemic subjects. *J. Clin. Invest.* **75:** 614–623.
8. Krul, E. S., K. G. Parhofer, P. H. R. Barrett, R. D. Wagner, and G. Schonfeld. 1992. ApoB-75, a truncation of apolipoprotein B associated with familial hypobetalipoproteinemia: genetic and kinetic studies. *J. Lipid Res.* **33:** 1037–1050.
9. Lindgren, F. T., L. C. Jensen, and F. T. Hatch. 1972. The isolation and quantitation analysis of serum lipoproteins. *In* Blood Lipid and Lipoproteins: Quantitation, Composition and Metabolism. G. J. Nelson, editor. Wiley-Interscience, New York. 181–274.
10. Stalenhoef, A. F. H., M. J. Malloy, J. P. Kane, and R. J. Havel. 1984. Metabolism of apolipoproteins B-48 and B-100 of triglyceride-rich lipoproteins in normal and lipoprotein lipase-deficient humans. *Proc. Natl. Acad. Sci. USA.* **81:** 1839–1843.
11. James, R. W., B. Martin, D. Pometta, J. C. Fruchart, P. Duriez, P. Puchois, J. P. Farriaux, A. Tacquet, T. Demant, R. J. Clegg, A. Munro, M. F. Oliver, C. J. Packard, and

J. Shepherd. 1989. Apolipoprotein B metabolism in homozygous familial hypercholesterolemia. *J. Lipid Res.* **30:** 159-169.

12. Demant, T., A. Gaw, G. F. Watts, P. Durrington, B. Buckley, C. W. Imrie, C. Wilson, C. J. Packard, and J. Shepherd. 1993. Metabolism of apoB-100-containing lipoproteins in familial hyperchylomicronemia. *J. Lipid Res.* **34:** 147-156.

13. Gaw, A., C. J. Packard, E. F. Murray, G. M. Lindsay, B. A. Griffin, M. J. Caslake, B. D. Vallance, A. R. Lorimer, and J. Shepherd. 1993. Effects of simvastatin on apoB metabolism and LDL subfraction distribution. *Arterioscler. Thromb.* **13:** 170-189.

14. Bilheimer, D. W., S. Eisenberg, and R. I. Levy. 1982. The metabolism of very low density lipoproteins, I. Preliminary in vitro and in vivo observations. *Biochim. Biophys. Acta.* **260:** 212-221.

15. Kane, J. P., T. Sata, R. L. Hamilton, and R. J. Havel. 1975. Apoprotein composition of very low density lipoproteins of human serum. *J. Clin. Invest.* **56:** 1622-1634.

16. Lowry, O. H., N. J. Rosebrough, A. L. Farr, and R. J. Randall. 1951. Protein measurement with the Folin phenol reagent. *J. Biol. Chem.* **193:** 265-275.

17. Lipid Research Clinics Program Manual of Laboratory Operations. 1975. DHEW Publications, No. (NIH) 75-628, Washington, DC.

18. Berman, M., and M. F. Weiss. 1974. SAAM Manual. Washington, DC, US Government Printing Office, United States Public Health Service publication No. 1703.

19. Packard, C. J., J. Shepherd, G. M. Lindsay, A. Gaw, and M-R. Taskinen. 1993. Thyroid replacement therapy and its influence on post-heparin plasma lipases and apolipoprotein B metabolism in hypothyroidism. *J. Clin. Endocrinol. Metab.* **76:** 1209-1216.

20. Packard, C. J., R. J. Clegg, M. H. Dominiczak, A. R. Lorimer, and J. Shepherd. 1986. Effects of bezafibrate on apolipoprotein B metabolism in type III hyperlipoproteinemic subjects. *J. Lipid Res.* **27:** 930-938.

21. Foster, D. M., A. Chait, J. J. Albers, R. A. Failor, C. Harris, and J. D. Brunzell. 1986. Evidence for kinetic heterogeneity among low density lipoproteins. *Metabolism.* **35:** 685-696.

22. Demant, T., D. Bedford, C. J. Packard, and J. Shepherd. 1991. The influence of apolipoprotein E polymorphism on apolipoprotein B-100 metabolism in normolipemic subjects. *J. Clin. Invest.* **88:** 1490-1501.

23. Langer, T., W. Strober, and R. I. Levy. 1972. The metabolism of low-density lipoprotein in familial type II hyperlipoproteinemia. *J. Clin. Invest.* **51:** 1528-1536.

24. Matthews, C. M. E. 1957. The theory of tracer experiments with ^{131}I-labeled plasma proteins. *Phys. Med. Biol.* **2:** 36-53.

25. Boston, R. C., P. C. Grief, and M. Berman. 1982. CONSAM. *In* Lipoprotein Kinetics and Modeling. M. Berman, S. M. Grundy, and B. V. Howard, editors. Academic Press, New York. 437-460.

26. Caslake, M. J., C. J. Packard, J. J. Series, B. Yip, M. M. Dagen, and J. Shepherd. 1992. Plasma triglyceride and low density lipoprotein metabolism. *Eur. J. Clin. Invest.* **22:** 96-104.

27. Reichl, D. 1994. Extravascular circulation of lipoproteins: their role in reverse transport of cholesterol. *Atherosclerosis.* **105:** 117-129.

28. Fisher, W. R. 1982. Apoprotein B kinetics in man: concepts and questions. *In* Lipoprotein Kinetics and Modeling. M. Berman, S. M. Grundy, and B. V. Howard, editors. Academic Press, New York. 43-68.

29. Malmendier, C. L., C. Delcroix, and J-F. Lontie. 1989. Kinetics of a heterogeneous population of particles in the low density lipoprotein apolipoprotein B. *Atherosclerosis.* **80:** 91-100.

30. Gaw, A., C. J. Packard, G. M. Lindsay, B. A. Griffin, M. J. Caslake, A. R. Lorimer, and J. Shepherd. 1994. Overproduction of small very low density lipoproteins (S_f 20-60) in moderate hypercholesterolemia: relationships between apolipoprotein B kinetics and plasma lipoproteins. *J. Lipid Res.* **36:** 000-000.

31. Taskinen, M-R., C. J. Packard, and J. Shepherd. 1990. Effect of insulin therapy on metabolic fate of apolipoprotein B-containing lipoproteins in NIDDM. *Diabetes.* **39:** 1017-1027.

32. Musliner, T. A., C. Giotas, and R. M. Krauss. 1986. Presence of multiple subpopulations of lipoproteins of intermediate density in normal subjects. *Arteriosclerosis.* **6:** 79-87.